BARD Final Report IS-4982-16

Development of heat-pulse sensors for measuring fluxes of water and solutes under the root zone

Kamai, T. Agricultural Research Organization
Kluitenberg, G. J. Kansas State University KS
Ben-Gal, A. Agricultural Research Organization

Project award year: 2016
One year feasibility project

1. Overall summary and statistics

Abstract

The objectives defined for this study were to: (1) develop a heat-pulse sensor and a heat-transfer model for leaching measurement, and (2) conduct laboratory study of the sensor and the methodology to estimate leaching flux.

In this study we investigated the feasibility for estimating leachate fluxes with a newly designed heat-pulse (HP) sensor, combining water flux density (WFD) with electrical conductivity (EC) measurements in the same sensor. Whereas previous studies used the conventional heat pulse sensor for these measurements, the focus here was to estimate WFD with a robust sensor, appropriate for field settings, having thick-walled large-diameter probes that would minimize their flexing during and after installation and reduce associated errors.

The HP method for measuring WFD in one dimension is based on a three-rod arrangement, aligned in the direction of the flow (vertical for leaching). A heat pulse is released from a center rod and the temperature response is monitored with upstream (US) and downstream (DS) rods. Water moving through the soil caries heat with it, causing differences in temperature response at the US and DS locations. Appropriate theory (e.g., Ren et al., 2000) is then used to determine WFD from the differences in temperature response.

In this study, we have constructed sensors with large probes and developed numerical and analytical solutions for approximating the measurement. One-dimensional flow experiments were conducted with WFD ranging between 50 and 700 cm per day. A numerical model was developed to mimic the measurements, and also served for the evaluation of the analytical solution. For estimation WFD, and analytical model was developed to approximate heat transfer in this setting. The analytical solution was based on the work of Knight et al. (2012) and Knight et al. (2016), which suggests that the finite properties of the rods can be captured to a large extent by assuming them to be cylindrical perfect conductors.

We found that: (1) the sensor is sensitive for measuring WFD in the investigated range, (2) the numerical model well-represents the sensor measurement, and (2) the analytical approximation could be improved by accounting for water and heat flow divergence by the large rods.

Contribution of the collaboration

The collaboration was very successful from two key aspects. First, the development of the heat-pulse method relies on successful agreement between measurement and theory, and therefore it is important that the development of the sensor and the theory is done together. During the development, there were many discussions regarding the sensor design and the appropriate assumptions made in the model development. This enabled parallel development of both. Second, Kamai visited Kluitenberg and Knight in KSU for a short time to work together. The fundamental aspects were developed during this short time of close collaborative work.

Achievements

The main achievement is the demonstrated feasibility for measuring WFD with a robust HP sensor. The development is separated to three major parts:

A. The Rigid Heat Pulse (R-HP) Sensor

Sensors were constructed with four probes made from stainless-steel tubes, 2.38-mm in diameter and 40-mm long (Figure 1). Three of those probes were utilized for the HP method, equipped with heater wire (center) and thermistors (sides). The additional (forth) tube was added to complete a 4-electrode Wenner array for EC measurements. The construction of the sensors were similar to the ones reported in Kamai et al. (2015).

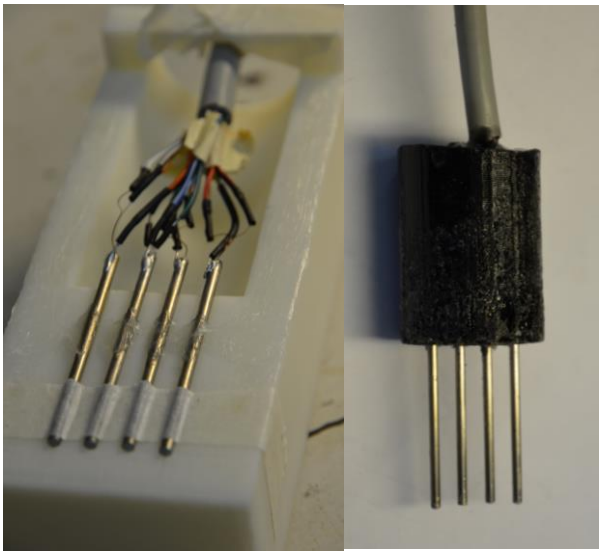

Figure 1. The fabricated R-HP sensor in the construction of the probes and their electrical connections (left), and after the cast of the sensor body epoxy (right).

B. Analytical solution for water flux density estimations

In this part, we capitalized on our previous models (Knight et al., 2012; Knight et al., 2016) and developed a solution for coupled water flow and heat transfer that accounts for the finite radius and finite thermal properties of the heater (emitter) and temperature-sensing (receiver) rods. The solution is in the Laplace domain, transformed numerically to the time domain, with details on the derivation and the solutions given in Appendix A. The solution is based on three simplifying assumptions: (i) the probes may be approximated as perfect conductor rods, (ii) water flow is considered unidirectional and parallel to the rod alignment, and (iii) there are no interactions between the rods. Please see Appendix A for further details and results.

C. Numerical model

The coupling of heat and water were simulated in a two-dimensional finite-element domain, using commercial software Comsol Multiphysics. With this model we aimed to capture the main physical properties and processes during measurements, neglecting the longitudinal dimension of the probes; thus, assuming infinite long probes without a sensor body. The model was designed

for simulating 5 different scenarios (Table 1) that were based on the complexity of the approximation of the probes' thermal properties and the water flow in the domain. The probes were either ignored (Scenario 1) or approximated either by perfect conductors or by two regions, mimicking the stainless-steel tubing filled with thermally conductive epoxy. The flow was approximated either by unidirectional flow, parallel to the rod alignment of the sensor, or by Darcy type flow that accounted for the flow around the rods. This enabled numerical simulations in different complexity levels, with: Scenario 1 – representing the ILS model; Scenario 2 – representing the developed analytical model; Scenario 3 – added complexity of water flow; Scenario 4 – added complexity of probes; and Scenario 5 – (the most complex) for mimicking the real sensor (without the 3rd dimension).

Table 1. Simulation scenarios for the numerical model

	Scenario 1	Scenario 2	Scenario 3	Scenario 4	Scenario 5
Water flow	Unidirectional	Unidirectional	Darcy	Unidirectional	Darcy
Probe region	No probes	PC	PC	Composite	Composite

By using this model together with the analytical models (ILS and the developed one), we identified the major assumptions and complexities that were necessary for accurate estimations. The results indicate that it is sufficient to assume the probes as perfect conductors and it is important to account for the water flow around the probes with a Darcy type flow, which are represented by Scenario 3. For further details and results, please refer to Appendix B.

Water flux density experiments and estimations

Prior to the WFD experiments, the sensor were immersed in immobilized water (4 g/l agar solution) for calibration of probe spacing. For the experiments, the sensors were installed in Plexiglas columns with the probes aligned in the column direction and penetrating from the side of the column. The column was filled with water and wet-packed with soil. The experimental setup was similar to Kamai et al. (2008), with the column connected to a peristaltic pump for establishing predetermined flow rates, verified by measuring the outflow rate. The experiments were conducted by establishing steady-state flow and executing several heat pulse measurements in 15-min intervals.

After temperature data collection, the analytical model was fit to the data, optimizing the volumetric heat capacity, thermal conductivity, and heat-pulse velocity, from which the WFD density was evaluated. Figure 2 depicts this procedure, presenting data and model fit from WFD of 200 cm/d. This is the method we used for estimating WFD from the measurements.

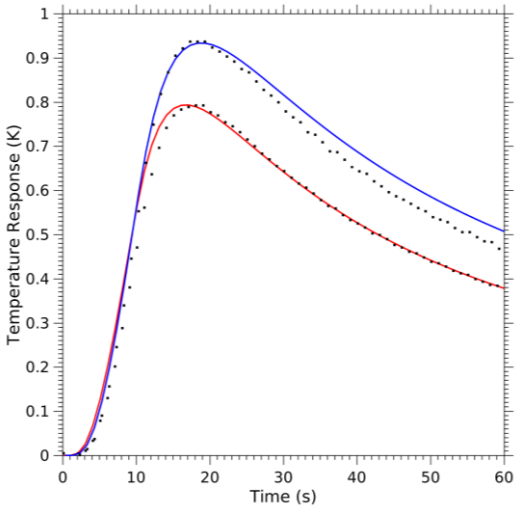

Figure 2. Measured (markers) and model-fit (lines) of upstream (red) and downstream (blue) temperature response curves with 200 cm per day WFD.

With this procedure we collected data and estimated WFD between 50 and 700 cm/d. Figure 3 depicts this range and the agreement between the applied WFD by the pump and the estimated flux from the HP method.

The results indicate that the general trend of WFD is captured with the method (Figure 3). Thus, the sensor is responding to different flux densities and that response is well-captured with the analytical model. The developed analytical solution that was used for the WFD estimations presented a significant improvement compared to the ILS model, which showed significant underestimation of WFD (results not presented). However, even with this new method, combining the sensor design and accompanied model, we still observe consistent underestimation of WFD, especially in the lower range (e.g., Figure 3). We attribute these underestimations to the lack of the analytical model to capture the flow divergence around the needle, which could be captured with the numerical model. Still, the results indicate on relatively accurate estimations of WFD with this new methodology.

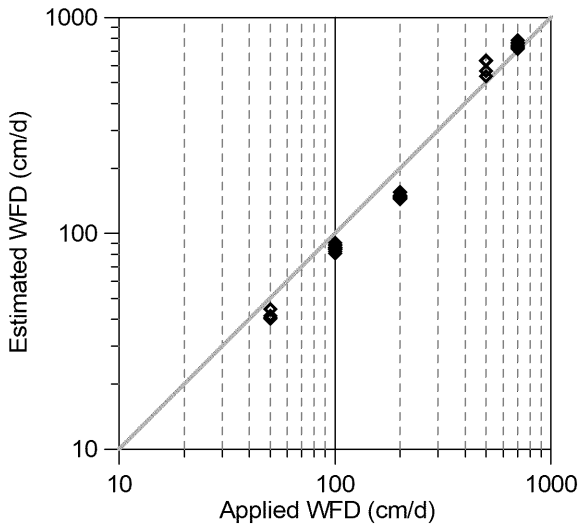

Figure 3. A subset from the experimental results comparing the applied and estimated WFD.

Publications for Project IS-4982-16

Status	Type	Authors	Title	Journal	Vol:pg Year	Coun

2. Appendices

Appendix A: A Semianalytical Solution for Transient Heat Transfer between Two Cylindrical Perfect Conductors in Porous Media with Uniform Darcy Flow

Introduction

Ren et al. (2000) developed a method for measuring soil water flux density. Measurements are made with a sensor that consists of three parallel, equally-spaced rods that lie in the same plane. The central emitter rod is used to introduce a heat pulse of finite duration. The receiver rods are used to measure the temperature rise at locations upstream and downstream from the emitter. Specifically, the method involves measuring the maximum difference between the temperature rise at the downstream and upstream locations. By using an appropriate solution of the heat equation, soil water flux density can determined from the maximum temperature difference, if the thermal properties of the medium and the rate and duration of heating are known. The line-source solution that Ren et al. (2000) used for this purpose does not account for the finite radius and finite thermal properties of the rods. In other words, it assumes that the rods have zero radius. It is appropriate to use this solution if the rods have radii that are small compared to their spacing, but no work has been done to determine the range of radius to spacing ratios for which this solution returns accurate flux measurements.

To address this issue, we need a version of the Ren et al. (2000) solution that accounts for the finite radius and finite thermal properties of the emitter and receiver rods. This is a tall order and likely would require the use of a numerical model; however, the work of Knight et al. (2012) suggests that the finite properties of the rods can be captured to a large extent by assuming them to be cylindrical perfect conductors. This report summarizes work done to derive a version of the Ren et al. (2000) solution that treats the three rods as cylindrical perfect conductors. We begin by

deriving the Laplace-domain solution for the temperature of the medium with only an emitter rod present. That solution is then used to obtain Laplace-domain solutions for the temperature of the receiver rods directly downstream and upstream from the emitter.

Problem Formulation

Consider a variably-saturated porous medium that is incompressible, homogeneous, isotropic, and infinite in extent. The porous medium is assumed to be stationary, but water is flowing through it at uniform velocity U_w parallel to the x axis. The bulk three-phase system has thermal conductivity λ , volumetric heat capacity C, and thermal diffusivity κ, with $\kappa = \lambda / C$. Assuming that the liquid and solid phases are in thermal equilibrium, and that the heat capacity of the gas phase is negligible, we have

$$U = U_w \frac{\vartheta C_w}{C} = J \frac{C_w}{C} \tag{1}$$

where U is the thermal front advection velocity (Melville et al., 1995), ϑ is the volumetric water content of the medium, C_w is the volumetric heat capacity of water, and J is the volumetric water flux density. The velocity U is a weighted average of the velocities of the water and the stationary porous medium (Marshall, 1958).

Embedded within the porous medium are two parallel rods that are infinite in length and have infinite thermal conductivity. The emitter rod has radius a_1 and volumetric heat capacity C_1; the receiver rod has radius a_2 and volumetric heat capacity C_2. The centerlines of the two rods are a distance L apart, with $(a_1 + a_2) = L$. We assume that the rods are in perfect thermal contact with the porous medium surrounding them. Let $V_1(t)$ and $V_2(t)$ be the temperatures of the emitter and

receiver rods, respectively. We derive a closed-form solution in the Laplace domain for $V_2(t)$, given an arbitrary heating function $\phi(t)$ for the emitter rod. The function $\phi(t)$ specifies the rate per unit length at which heat is released from the emitter rod.

As shown in Figure A1a, we use the coordinate system (x, y) with the emitter rod centered at $(x, y) = (0, 0)$ and the receiver rod centered at $(x, y) = (L, 0)$. We also use polar coordinate systems (r_1, θ_1) and (r_2, θ_2) centered on the emitter and receiver rods, respectively. The coordinates (r_1, θ_1) satisfy the conditions $r_1^2 = x^2 + y^2$ and $(x, y) = (r_1 \cos\theta_1, r_1 \sin\theta_1)$, and the coordinates (r_2, θ_2) satisfy the conditions $r_2^2 = (x-L)^2 + y^2$ and $(x-L, y) = (r_2 \cos\theta_2, r_2 \sin\theta_2)$.

The temperature of the medium, $\upsilon(x, y, t)$, satisfies the governing equation

$$\nabla^2 \upsilon - \frac{U}{\kappa}\frac{\partial \upsilon}{\partial x} - \frac{1}{\kappa}\frac{\partial \upsilon}{\partial t} = 0; \quad r_1 \geq a_1, r_2 \geq a_2 \tag{2}$$

and it remains bounded at zero in the limit as $x, y \to \infty$. The medium and both rods must also satisfy a zero-temperature initial condition. Although (2) is written in terms of the (x, y) coordinate system, the boundary conditions and energy balances are best expressed in terms of the polar coordinates (r_1, θ_1) and (r_2, θ_2), with the temperature of the medium denoted by $\upsilon(r_1, \theta_1, t)$ or $\upsilon(r_2, \theta_2, t)$. We assume that the rods are in perfect thermal contact with the medium, so the conditions to be satisfied at the surfaces of the two rods are

$$\upsilon(a_1, \theta_1, t) = V_1(t); \quad 0 \leq \theta_1 < 2\pi, t > 0 \tag{3}$$

$$\upsilon(a_2, \theta_2, t) = V_2(t); \quad 0 \leq \theta_2 < 2\pi, t > 0 \tag{4}$$

The energy balance for the emitter rod is

$$-a_1\lambda\int_0^{2\pi}\left.\frac{\partial\upsilon}{\partial r_1}\right|_{r_1=a_1} d\theta_1 = \phi(t) - \pi a_1^2 C_1 \frac{dV_1}{dt}\,; \quad t>0 \tag{5}$$

and the corresponding expression for the receiver rod is

$$-a_2\lambda\int_0^{2\pi}\left.\frac{\partial\upsilon}{\partial r_2}\right|_{r_2=a_2} d\theta_2 = -\pi a_2^2 C_2 \frac{dV_2}{dt}\,; \quad t>0 \tag{6}$$

The left-hand sides of (5) and (6) are the total flux of heat per unit length into the medium from the emitter and receiver rods, respectively. The convective component of the heat flux vanishes from these energy balances because boundary conditions (3) and (4) impose constant temperatures everywhere on the boundaries $r_1 = a_1$ and $r_2 = a_2$. Thus, at any point on the upstream portions of boundaries $r_1 = a_1$ and $r_2 = a_2$, the radial component of the heat flux per unit length is identical to the radial component of the heat flux at the corresponding point on the downstream portions of boundaries $r_1 = a_1$ and $r_2 = a_2$. In other words, for both rods, the flux per unit length entering the rod via convection is identical to the flux per unit length exiting it via convection.

Transformation of the Governing Equation and Side Conditions

This problem can be solved by introducing the modified temperature *u*, defined by $u \equiv \upsilon\exp(-bx)$, with $b = U/(2\kappa)$. The utility of this transformation is that the governing equation simplifies to

$$\nabla^2 u - b^2 u - \frac{1}{\kappa}\frac{\partial u}{\partial t} = 0\,; \quad r_1 \geq a_1, r_2 \geq a_2 \tag{7}$$

In terms of the two sets of polar coordinates, the modified temperature is expressed as

$$u(r_1,\theta_1,t) \equiv \upsilon(r_1,\theta_1,t)\exp(-br_1\cos\theta_1) \tag{8}$$

$$u(r_2,\theta_2,t) \equiv \upsilon(r_2,\theta_2,t)\exp(-bL)\exp(-br_2\cos\theta_2) \tag{9}$$

so the boundary conditions become

$$u(a_1,\theta_1,t) = V_1(t)\,e^{-ba_1\cos\theta_1}\ ; \quad 0 \le \theta_1 < 2\pi,\ t > 0 \tag{10}$$

$$u(a_2,\theta_2,t) = V_2(t)\,e^{-bL}e^{-ba_2\cos\theta_2}\ ; \quad 0 \le \theta_2 < 2\pi,\ t > 0 \tag{11}$$

and the energy balance expressions for the emitter and receiver rods become

$$-a_1\lambda\int_0^{2\pi} e^{ba_1\cos\theta_1}\left.\frac{\partial u}{\partial r_1}\right|_{r_1=a_1} d\theta_1 = \phi(t) - \pi a_1^2 C_1\frac{dV_1}{dt}\ ; \quad t > 0 \tag{12}$$

$$-a_2\lambda e^{bL}\int_0^{2\pi} e^{ba_2\cos\theta_2}\left.\frac{\partial u}{\partial r_2}\right|_{r_2=a_2} d\theta_2 = -\pi a_2^2 C_2\frac{dV_2}{dt}\ ; \quad t > 0 \tag{13}$$

The transformation employed here has no effect on the initial condition or the boundedness condition. Thus, like the original temperature υ, the modified temperature u satisfies a zero-temperature initial condition and it remains bounded at zero as $x, y \to \infty$.

The Problem in the Laplace Domain

We solve this problem in terms of functions in the Laplace transform domain, making use of the definition

$$\hat{f}(p) \equiv \int_0^{\infty} f(t)\exp(-pt)\,dt \tag{14}$$

where $\hat{f}(p)$ is the Laplace transform of the function $f(t)$ and p is the transform variable. Taking the Laplace transform of (7) and satisfying the zero initial condition yields the subsidiary equation

$$\nabla^2 \hat{u} - \mu^2 \hat{u} = 0\,; \quad r_1 \geq a_1, r_2 \geq a_2 \tag{15}$$

with $\mu^2 = b^2 + p/\kappa$. Likewise, taking the Laplace transforms of (10) and (11) yields the boundary conditions

$$\hat{u}(a_1, \theta_1, p) = \hat{V}_1(p) e^{-ba_1 \cos\theta_1}\,; \quad 0 \leq \theta_1 < 2\pi \tag{16}$$

$$\hat{u}(a_2, \theta_2, p) = \hat{V}_2(p) e^{-bL} e^{-ba_2 \cos\theta_2}\,; \quad 0 \leq \theta_2 < 2\pi \tag{17}$$

and the Laplace transforms of the energy balance expressions are

$$-a_1 \lambda \int_0^{2\pi} e^{ba_1 \cos\theta_1} \left.\frac{\partial \hat{u}}{\partial r_1}\right|_{r_1 = a_1} d\theta_1 = \hat{\phi}(p) - \pi a_1^2 C_1 p \hat{V}_1(p) \tag{18}$$

$$-a_2 \lambda e^{bL} \int_0^{2\pi} e^{ba_2 \cos\theta_2} \left.\frac{\partial \hat{u}}{\partial r_2}\right|_{r_2 = a_2} d\theta_2 = -\pi a_2^2 C_2 p \hat{V}_2(p) \tag{19}$$

Like the original temperature υ and the modified temperature u, the Laplace transform of the modified temperature remains bounded at zero as $x, y \to \infty$.

Solution Centered at the Emitter

The general solution of (15) that satisfies the boundedness condition is (Carslaw and Jaeger, 1959, p. 390)

$$\hat{u}(r_1, \theta_1, p) = \sum_{n=0}^{\infty} c_n K_n(\mu r_1) \cos(n\theta_1) \tag{20}$$

where $K_n(\ )$ is the modified Bessel function of the second kind and order *n*. The coefficients c_n in this solution are determined by satisfying boundary condition (16). This is accomplished by using the expansion (Olver, 1965, p. 376)

$$e^{-br_1\cos\theta_1} \equiv \sum_{n=0}^{\infty}(-1)^n \varepsilon_n I_n(br_1)\cos(n\theta_1) \tag{21}$$

where $\varepsilon_0 \equiv 1,\ \varepsilon_n \equiv 2$ for $n \geq 1$, and $I_n(\ )$ is the modified Bessel function of the first kind and order *n*. The coefficients c_n are determined by using (21) to write boundary condition (16) as an infinite series, and it follows that the solution in the Laplace domain is

$$\hat{u}(r_1,\theta_1,p) = \hat{V}_1(p)\sum_{n=0}^{\infty}\frac{(-1)^n\varepsilon_n I_n(ba_1)K_n(\mu r_1)}{K_n(\mu a_1)}\cos(n\theta_1);\quad r_1 \geq a_1 \tag{22}$$

where $\hat{V}_1(p)$ is to be determined by satisfying (18), the energy balance for the emitter rod.

The derivative in (18) is obtained by differentiating (22) to yield the expression

$$\frac{\partial\hat{u}}{\partial r_1} = \frac{1}{r_1}\hat{V}_1(p)\sum_{n=0}^{\infty}\frac{(-1)^n\varepsilon_n I_n(ba_1)}{K_n(\mu a_1)}[nK_n(\mu r_1) - \mu r_1 K_{n+1}(\mu r_1)]\cos(n\theta_1) \tag{23}$$

and the integral in (18) can then be evaluated by using equation (9.6.19) of Olver (1965). Thus, we see that (18) becomes

$$2\pi\lambda\hat{V}_1(p)\sum_{n=0}^{\infty}\frac{(-1)^n\varepsilon_n I_n(ba_1)}{K_n(\mu a_1)}[\mu a_1 K_{n+1}(\mu a_1) - nK_n(\mu a_1)] = \hat{\phi}(p) - \pi a_1^2 C_1 p\hat{V}_1(p) \tag{24}$$

and the Laplace transform of the temperature of the emitter rod can therefore be written as

$$\hat{V}_1(p) = \frac{\hat{\phi}(p)}{2\pi\lambda W_1} \tag{25}$$

with

$$W_1(p) = \frac{a_1^2 \beta_1 p}{2\kappa} + \sum_{n=0}^{\infty} \frac{(-1)^n \varepsilon_n I_n^2(ba_1)}{K_n(\mu a_1)} [\mu a_1 K_{n+1}(\mu a_1) - nK_n(\mu a_1)] \tag{26}$$

and $\beta_1 = C_1/C$.

Substituting the expression for $\hat{V}_1(p)$ into (22) yields the desired solution

$$\hat{u}(r_1, \theta_1, p) = \frac{\hat{\phi}(p)}{2\pi\lambda W_1} \sum_{n=0}^{\infty} \frac{(-1)^n \varepsilon_n I_n(ba_1) K_n(\mu r_1)}{K_n(\mu a_1)} \cos(n\theta_1); \quad r_1 \geq a_1 \tag{27}$$

for the Laplace transform of the modified temperature of the medium. This solution is used in the next section to derive an expression for $\hat{V}_2(p)$. The Laplace-domain solution for the original temperature is obtained by substituting (22) into the expression $\hat{\upsilon}(r_1, \theta_1, p) = \hat{u}(r_1, \theta_1, p) e^{br_1 \cos\theta_1}$, which is obtained by taking the Laplace transform of (8). Thus, we see that

$$\hat{\upsilon}(r_1, \theta_1, p) = e^{br_1 \cos\theta_1} \frac{\hat{\phi}(p)}{2\pi\lambda W_1} \sum_{n=0}^{\infty} \frac{(-1)^n \varepsilon_n I_n(ba_1) K_n(\mu r_1)}{K_n(\mu a_1)} \cos(n\theta_1); \quad r_1 \geq a_1 \tag{28}$$

We do not explicitly make use of this solution, but it is useful for showing that the theory presented here is consistent with existing solutions. In the limit as $U \to 0$, the expressions for $\hat{V}_1(p)$ and $\hat{\upsilon}(r_1, \theta_1, p)$ reduce to equations (15) and (16), respectively, of Knight et al. (2012). And, in the limit as $a_1 \to 0$, solution (28) simplifies to

$$\hat{\upsilon}(r_1, \theta_1, p) = e^{br_1 \cos\theta_1} \frac{\hat{\phi}(p)}{2\pi\lambda} K_0(\mu r_1) \tag{29}$$

which is the Laplace transform of the well-known solution for a moving line source (Carslaw and Jaeger, 1959, p. 261).

Solution Centered at the Receiver

The same approach used to derive (27) can be used to show that the solution of (15) satisfying boundary condition (17) is

$$\hat{u}(r_2,\theta_2,p)=\hat{V}_2(p)e^{-bL}\sum_{n=0}^{\infty}\frac{(-1)^n\varepsilon_n I_n(ba_2)K_n(\mu r_2)}{K_n(\mu a_2)}\cos(n\theta_2);\quad r_2\geq a_2 \tag{30}$$

This solution has essentially the same form as the expression for $\hat{u}(r_1,\theta_1,p)$, but differs by a factor of $\exp(-bL)$. At the receiver rod we therefore look for a solution of the form

$$\begin{aligned}\hat{u}(r_2,\theta_2,p)=\hat{V}_2(p)e^{-bL}&\sum_{n=0}^{\infty}\frac{(-1)^n\varepsilon_n I_n(ba_2)K_n(\mu r_2)}{K_n(\mu a_2)}\cos(n\theta_2)\\&+\frac{\hat{\phi}(p)}{2\pi\lambda W_1}\sum_{n=0}^{\infty}\frac{(-1)^n\varepsilon_n I_n(ba_1)K_n(\mu r_1)}{K_n(\mu a_1)}\cos(n\theta_1)\\&-\sum_{m=-\infty}^{\infty}(-1)^m d_m K_m(\mu r_2)\cos(m\theta_2)\end{aligned} \tag{31}$$

where the coefficients d_m are to be determined by satisfying boundary condition (17). This is accomplished by using the addition theorem

$$K_n(\mu r_1)\cos(n\theta_1)=\sum_{m=-\infty}^{\infty}(-1)^m K_{n+m}(\mu L)I_m(\mu r_2)\cos(m\theta_2) \tag{32}$$

which is equation (43) of Knight et al. (2016) rewritten in terms of dimensioned variables. Use of this addition theorem allows us to write (31) in the form

$$\begin{aligned}\hat{u}(r_2,\theta_2,p)=\hat{V}_2(p)e^{-bL}&\sum_{n=0}^{\infty}\frac{(-1)^n\varepsilon_n I_n(ba_2)K_n(\mu r_2)}{K_n(\mu a_2)}\cos(n\theta_2)\\+\frac{\hat{\phi}(p)}{2\pi\lambda W_1}&\sum_{n=0}^{\infty}\frac{(-1)^n\varepsilon_n I_n(ba_1)}{K_n(\mu a_1)}\left[\sum_{m=-\infty}^{\infty}(-1)^m K_{n+m}(\mu L)I_m(\mu r_2)\cos(m\theta_2)\right]\\&-\sum_{m=-\infty}^{\infty}(-1)^m d_m K_m(\mu r_2)\cos(m\theta_2)\end{aligned} \tag{33}$$

After reversing the order of summation in the second term of this expression, we put $r_2 = a_2$ and use boundary condition (17) and the expansion

$$e^{-ba_2\cos\theta_2} \equiv \sum_{n=0}^{\infty}(-1)^n \varepsilon_n I_n(ba_2)\cos(n\theta_2) \tag{34}$$

to find that the coefficients are

$$d_m = \frac{\hat{\phi}(p)}{2\pi\lambda W_1}\frac{I_m(\mu a_2)}{K_m(\mu a_2)}\sum_{n=0}^{\infty}\frac{(-1)^n \varepsilon_n I_n(ba_1)K_{n+m}(\mu L)}{K_n(\mu a_1)} \tag{35}$$

Thus, it follows that (33) becomes

$$\begin{aligned}\hat{u}(r_2,\theta_2,p) &= \hat{V}_2(p)e^{-bL}\sum_{n=0}^{\infty}\frac{(-1)^n \varepsilon_n I_n(ba_2)K_n(\mu r_2)}{K_n(\mu a_2)}\cos(n\theta_2)\\ &+\frac{\hat{\phi}(p)}{2\pi\lambda W_1}\sum_{m=-\infty}^{\infty}\left[\sum_{n=0}^{\infty}\frac{(-1)^n \varepsilon_n I_n(ba_1)K_{n+m}(\mu L)}{K_n(\mu a_1)}\right](-1)^m I_m(\mu r_2)\cos(m\theta_2)\\ &-\frac{\hat{\phi}(p)}{2\pi\lambda W_1}\sum_{m=-\infty}^{\infty}\left[\sum_{n=0}^{\infty}\frac{(-1)^n \varepsilon_n I_n(ba_1)K_{n+m}(\mu L)}{K_n(\mu a_1)}\right]\frac{(-1)^m I_m(\mu a_2)K_m(\mu r_2)}{K_m(\mu a_2)}\cos(m\theta_2)\end{aligned} \tag{36}$$

where $\hat{V}_2(p)$ is to be determined by satisfying (19), the energy balance for the receiver rod.

The derivative in (19) is complicated, but at $r_2 = a_2$ it simplifies to

$$\begin{aligned}\left.\frac{\partial\hat{u}}{\partial r_2}\right|_{r_2=a_2} &= \frac{1}{a_2}\hat{V}_2(p)e^{-bL}\sum_{n=0}^{\infty}\frac{(-1)^n \varepsilon_n I_n(ba_2)}{K_n(\mu a_2)}[nK_n(\mu a_2)-\mu a_2 K_{n+1}(\mu a_2)]\cos(n\theta_2)\\ &+\frac{1}{a_2}\frac{\hat{\phi}(p)}{2\pi\lambda W_1}\sum_{m=-\infty}^{\infty}\left[\sum_{n=0}^{\infty}\frac{(-1)^n \varepsilon_n I_n(ba_1)K_{n+m}(\mu L)}{K_n(\mu a_1)}\right]\frac{(-1)^m\cos(m\theta_2)}{K_m(\mu a_2)}\end{aligned} \tag{37}$$

by making use of the Wronskian relation (Olver, 1965, p. 375). We now substitute this result into (19) and integrate to obtain the expression

$$\pi a_2^2 C_2 p\hat{V}_2(p) = 2\pi\lambda\hat{V}_2(p)\sum_{n=0}^{\infty}\frac{(-1)^n\varepsilon_n I_n^2(ba_2)}{K_n(\mu a_2)}[nK_n(\mu a_2)-\mu a_2 K_{n+1}(\mu a_2)] + \frac{\hat{\phi}(p)}{W_1}e^{bL}\sum_{m=-\infty}^{\infty}\left[\sum_{n=0}^{\infty}\frac{(-1)^n\varepsilon_n I_n(ba_1)K_{n+m}(\mu L)}{K_n(\mu a_1)}\right]\frac{(-1)^m I_m(ba_2)}{K_m(\mu a_2)} \tag{38}$$

After rearranging the second term in this expression so that summation on *m* begins with *m* = 0, we find that the Laplace transform of the receiver rod temperature can be written as

$$\hat{V}_2(p) = \frac{\hat{\phi}(p)W_{12}}{4\pi\lambda W_1 W_2}\exp(bL) \tag{39}$$

where W_1 is the expression from (26). We also have

$$W_2(p) = \frac{a_2^2\beta_2 p}{2\kappa} + \sum_{n=0}^{\infty}\frac{(-1)^n\varepsilon_n I_n^2(ba_2)}{K_n(\mu a_2)}[\mu a_2 K_{n+1}(\mu a_2) - nK_n(\mu a_2)] \tag{40}$$

$$W_{12}(p) = \sum_{m=0}^{\infty}\left\{\sum_{n=0}^{\infty}\frac{(-1)^n\varepsilon_n I_n(ba_1)[K_{n-m}(\mu L)+K_{n+m}(\mu L)]}{K_n(\mu a_1)}\right\}\frac{(-1)^m\varepsilon_m I_m(ba_2)}{K_m(\mu a_2)} \tag{41}$$

in which $\beta_2 = C_2/C$, $\varepsilon_0 \equiv 1$, and $\varepsilon_m \equiv 2$ for $m \geq 1$. The expression for $\hat{V}_2(p)$ can be substituted into (36) to obtain expressions centered at the receiver rod for the modified temperature and original temperature of the medium, but we do not present those results here.

In the limit as $U \to 0$, the expression for $\hat{V}_2(p)$ reduces to equation (35) of Knight et al. (2012). In the limit as $a_2 \to 0$, it simplifies to

$$\hat{V}_2(p) = \frac{\hat{\phi}(p)}{2\pi\lambda W_1}e^{bL}\sum_{n=0}^{\infty}\frac{(-1)^n\varepsilon_n I_n(ba_1)K_n(\mu L)}{K_n(\mu a_1)} \tag{42}$$

which is identical to equation (28) evaluated at $(r_1, \theta_1) = (L, 0)$, the location at which the receiver is centered. It is also of interest to consider the limiting behavior of solution (39) as $a_1 \to 0$. In this case we find that

$$\hat{V}_2(p) = \frac{\hat{\phi}(p)}{2\pi\lambda W_2} e^{bL} \sum_{m=0}^{\infty} \frac{(-1)^m \varepsilon_m I_m(ba_2) K_m(\mu L)}{K_m(\mu a_2)} \tag{43}$$

This expression is identical in form to (42), so we conclude that, if the emitter and receiver rods have identical properties, the finite radius and finite heat capacity of the receiver have the same effect on the receiver temperature as the finite radius and finite heat capacity of emitter rod. In the limit as $a_1, a_2 \to 0$, solution (39) simplifies to

$$\hat{V}_2(p) = \frac{\hat{\phi}(p)}{2\pi\lambda} K_0(\mu L) \exp(bL) \tag{44}$$

which is identical to (29) evaluated at $(r_1, \theta_1) = (L, 0)$. This line-source solution gives the Laplace transform of the temperature of the receiver rods for the case where the emitter and receiver rods both have zero radius and zero heat capacity.

For the case of zero flow, Knight et al. (2012) showed that the solution for $\hat{V}_2(p)$ can be expressed as the product of three quantities: a transfer function for the emitter rod, a transfer function for the receiver rod, and the Laplace transform of the line-source solution evaluated at the location of the receiver rod. Comparing the forms of (39) and (44) reveals that such an approach does not hold for the case of $U > 0$.

Solution for an Upstream Receiver

To this point we have considered only the case where the receiver rod is located directly downstream from the emitter rod. However, if the problem is solved with the flow direction reversed (i.e., using a thermal front advection velocity of $-U$ instead of U), the solution corresponds to the case where the receiver rod is located a distance L directly upstream from the emitter rod (Figure A1b). Reversing the direction of flow has no effect on the temperature of the emitter rod because, as noted earlier, we assume that the temperature distribution in the vicinity of the emitter is unaffected by the presence of the receiver rod.

Results for the upstream receiver rod are presented by using a_3 for its radius, C_3 for is its volumetric heat capacity, and $V_3(t)$ for its temperature. In terms of these variables we have

$$\hat{V}_3(p) = \frac{\hat{\phi}(p) W_{13}}{4\pi\lambda W_1 W_3} \exp(-bL) \tag{45}$$

with

$$W_3(p) = \frac{a_3^2 \beta_3 p}{2\kappa} + \sum_{n=0}^{\infty} \frac{(-1)^n \varepsilon_n I_n^2(ba_3)}{K_n(\mu a_3)} [\mu a_3 K_{n+1}(\mu a_3) - n K_n(\mu a_3)] \tag{46}$$

$$W_{13}(p) = \sum_{m=0}^{\infty} \left\{ \sum_{n=0}^{\infty} \frac{\varepsilon_n I_n(ba_1)[K_{n-m}(\mu L) + K_{n+m}(\mu L)]}{K_n(\mu a_1)} \right\} \frac{\varepsilon_m I_m(ba_3)}{K_m(\mu a_3)} \tag{47}$$

where $\beta_3 = C_3/C$ and W_1 is identical to the expression for W_1 in equation (26). Notice that W_{13} is similar in form to the expression for W_{12} in (41), but does not contain the factors of $(-1)^n$ and $(-1)^m$.

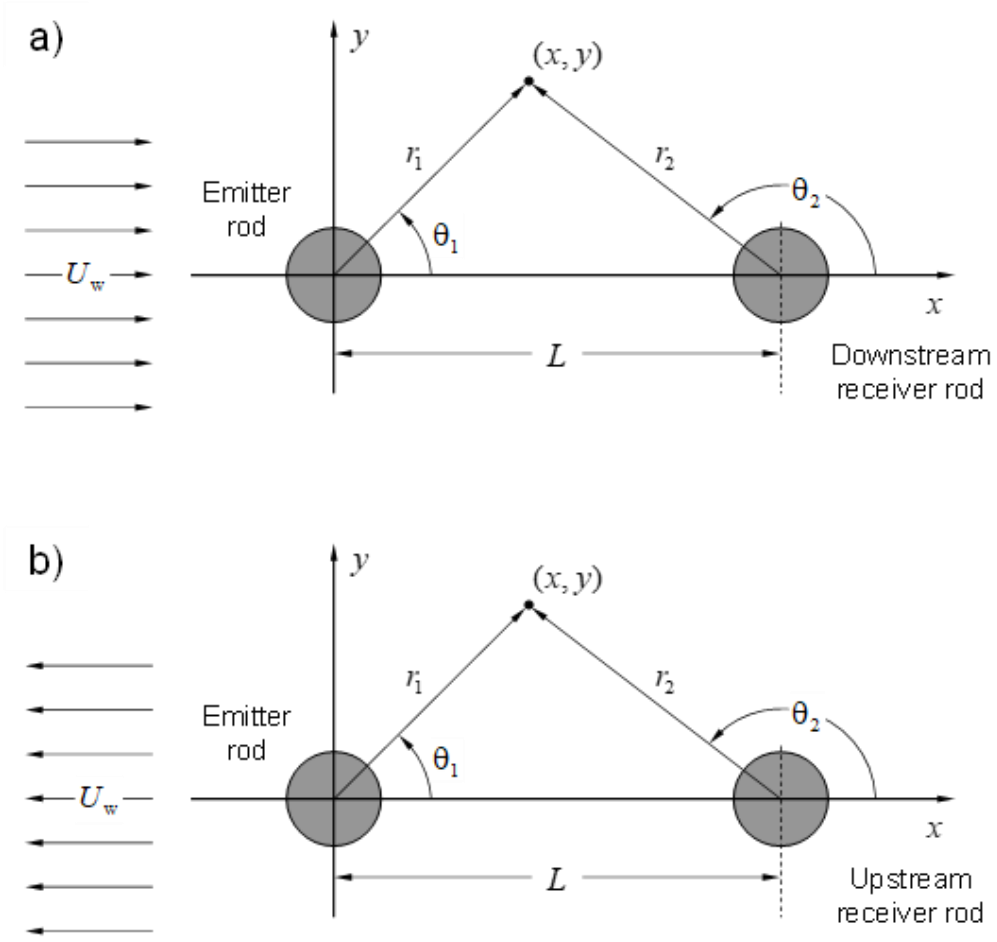

Figure A1. Coordinate systems used in the derivation of the solution for cases where water moves with a) uniform velocity U_w and b) uniform velocity $-U_w$. The Cartesian coordinate system (x, y) is centered on the emitter rod at $(x, y) = (0, 0)$, and the distance from the emitter rod is r_1, satisfying $r_1^2 = x^2 + y^2$. The receiver rod is centered at $(x, y) = (L, 0)$, so the distance from the receiver rod is r_2, satisfying $r_2^2 = (x - L)^2 + y^2$. Also shown are polar coordinate systems (r_1, θ_1) and (r_2, θ_2) centered on the emitter and receiver rods, respectively, where $(x, y) = (r_1 \cos\theta_1, r_1 \sin\theta_1)$ and $(x - L, y) = (r_2 \cos\theta_2, r_2 \sin\theta_2)$.

In the limit as $U \to 0$, the expression for $\hat{V}_3(p)$ reduces to equation (35) of Knight et al. (2012). In the limit as $a_3 \to 0$, it simplifies to

$$\hat{V}_3(p) = \frac{\hat{\phi}(p)}{2\pi\lambda W_1} e^{-bL} \sum_{n=0}^{\infty} \frac{\varepsilon_n I_n(ba_1) K_n(\mu L)}{K_n(\mu a_1)} \tag{48}$$

It is also of interest to consider the limiting behavior of solution (45) as $a_1 \to 0$. In this case we find that

$$\hat{V}_3(p) = \frac{\hat{\phi}(p)}{2\pi\lambda W_3} e^{-bL} \sum_{m=0}^{\infty} \frac{\varepsilon_m I_m(ba_3) K_m(\mu L)}{K_m(\mu a_3)} \tag{49}$$

This expression is identical in form to (48), so we conclude that, if the emitter and receiver rods have identical properties, the finite radius and finite heat capacity of the receiver rod have the same effect on the receiver rod temperature as the finite radius and finite heat capacity of emitter rod. In the limit as $a_1, a_3 \to 0$, solution (45) simplifies to

$$\hat{V}_3(p) = \frac{\hat{\phi}(p)}{2\pi\lambda} K_0(\mu L) \exp(-bL) \tag{50}$$

which gives the Laplace transform of the temperature of the upstream receiver rod for the case where the emitter and upstream receiver rods both have zero radius and zero heat capacity.

Special Case of the Solutions for a Heat Pulse of Finite Duration

The expressions for $\hat{V}_2(p)$ and $\hat{V}_3(p)$ are general solutions in that they are written in terms of $\hat{\phi}(p)$, the Laplace transform of the arbitrary heating function. Here we present specific solutions for $V_2(t)$ and $V_3(t)$ for the special case where heat is released from the emitter rod at a constant rate for a finite period of time. The heating function is written as

$$\phi(t) = \begin{cases} q'; & 0 < t \le t_0 \\ 0; & t > t_0 \end{cases} \tag{51}$$

where t_0 is the duration of heating and q' is the rate per unit length at which heat is released from the emitter rod. The Laplace transform of this function is $\hat{\phi}(p) = q'p^{-1}[1-\exp(pt_0)]$, but it is best not to use this result to evaluate (39) and (45). Better accuracy can be achieved by inverting (39) and (45) numerically for the case of continuous heating. Results for heating of finite duration can then be obtained from the continuous heating results by employing the principle of superposition, with a time shift, in the time domain. Formally, this involves writing (39) as

$$\hat{V}_2^{\mathrm{C}}(p) = \frac{q'W_{12}}{4\pi\lambda p W_1 W_2}\exp(bL) \tag{52a}$$

which is inverted numerically to obtain values of $V_2^{\mathrm{C}}(t)$ and $V_2^{\mathrm{C}}(t-t_0)$ for times *t* of interest. These results are then substituted into the expression

$$V_2(t) = \begin{cases} V_2^{\mathrm{C}}(t); & 0 < t \le t_0 \\ V_2^{\mathrm{C}}(t) - V_2^{\mathrm{C}}(t-t_0); & t > t_0 \end{cases} \tag{52b}$$

to get the rod temperature corresponding to heating of finite duration. The corresponding expressions for evaluating (45) are

$$\hat{V}_3^{\mathrm{C}}(p) = \frac{q'W_{13}}{4\pi\lambda p W_1 W_3}\exp(-bL) \tag{53a}$$

$$V_3(t) = \begin{cases} V_3^{\mathrm{C}}(t); & 0 < t \le t_0 \\ V_3^{\mathrm{C}}(t) - V_3^{\mathrm{C}}(t-t_0); & t > t_0 \end{cases} \tag{53b}$$

For the limiting case where the emitter and both receiver rods have zero radius and zero heat capacity, we can replace (52a) with the simpler expression

$$\hat{V}_2^{\mathrm{C}}(p) = \frac{q'}{2\pi\lambda p}K_0(\mu L)\exp(bL) \tag{54}$$

which originates from the line source solution (44). Likewise, we can replace (53a) with the simpler expression

$$\hat{V}_3^{\mathrm{C}}(p) = \frac{q'}{2\pi\lambda p} K_0(\mu L)\exp(-bL) \tag{55}$$

which originates from the line source solution (50).

Numerical inversion of (52a), (53a), (54), and (55) was accomplished by using the algorithm of Stehfest (1970a, 1970b) with 16 coefficients. Details of the numerical inversion procedure and values for the 16 coefficients are provided in Appendix B of Knight et al. (2012). Computations were performed with MATLAB (version 8.4, The MathWorks), and the modified Bessel functions of the first and second kind were evaluated with the built-in functions BESSELI and BESSELK, respectively. The expressions for W_1, W_2, W_3, W_{12}, and W_{13} were evaluated with the first nine terms of the infinite series; however, the series in these expressions converge extremely rapidly. Convergence is most rapid for small values of *b*, which correspond to small flow rates, but even for the largest value of *b* used in this work, results correct to four decimal places can be achieved by evaluating only the first two terms of the infinite series in W_1, W_2, W_3, W_{12}, and W_{13}.

The Solutions in Dimensionless Form

The Laplace transforms of $V_2(t)$ and $V_3(t)$ can be written in dimensionless form by using $\tau = \kappa t/L^2$ for dimensionless time; $\tau_0 = \kappa t_0/L^2$ for dimensionless heating duration; and $\alpha_1 = a_1/L$, $\alpha_2 = a_2/L$, and $\alpha_3 = a_3/L$ for the dimensionless radii of the three rods. Dimensionless forms for the temperature of the downstream and upstream receiver rods are $\Theta_2(\tau) = CL^2V_2/(q't_0)$ and $\Theta_3(\tau) = CL^2V_3/(q't_0)$, respectively. We also define the dimensionless quantities $B = bL = UL/(2\kappa)$, $\xi = \mu L$, and $s = pL^2/\kappa$, where *s* is the dimensionless equivalent of Laplace transform parameter *p*. And the dimensionless equivalent of the relationship $\mu^2 = b^2 + p/\kappa$ is $\xi^2 = B^2 + s$.

In terms of these variables, expressions (52a) and (52b) take the form

$$\hat{\Theta}_2^{\mathrm{C}}(s) = \frac{Z_{12}}{4\pi\tau_0 s Z_1 Z_2}\exp(B) \tag{56a}$$

$$\Theta_2(\tau) = \begin{cases} \Theta_2^{\mathrm{C}}(\tau); & 0 < \tau \le \tau_0 \\ \Theta_2^{\mathrm{C}}(\tau) - \Theta_2^{\mathrm{C}}(\tau - \tau_0); & \tau > \tau_0 \end{cases} \tag{56b}$$

and expressions (53a) and (53b) take the form

$$\hat{\Theta}_3^{\mathrm{C}}(s) = \frac{Z_{13}}{4\pi\tau_0 s Z_1 Z_3}\exp(-B) \tag{57a}$$

$$\Theta_3(\tau) = \begin{cases} \Theta_3^{\mathrm{C}}(\tau); & 0 < \tau \le \tau_0 \\ \Theta_3^{\mathrm{C}}(\tau) - \Theta_3^{\mathrm{C}}(\tau - \tau_0); & \tau > \tau_0 \end{cases} \tag{57b}$$

with

$$Z_1(s) = \frac{\alpha_1^2\beta_1 s}{2} + \sum_{n=0}^{\infty}\frac{(-1)^n\varepsilon_n I_n^2(B\alpha_1)}{K_n(\xi\alpha_1)}[\xi\alpha_1 K_{n+1}(\xi\alpha_1) - nK_n(\xi\alpha_1)] \tag{58}$$

$$Z_2(s) = \frac{\alpha_2^2\beta_2 s}{2} + \sum_{n=0}^{\infty}\frac{(-1)^n\varepsilon_n I_n^2(B\alpha_2)}{K_n(\xi\alpha_2)}[\xi\alpha_2 K_{n+1}(\xi\alpha_2) - nK_n(\xi\alpha_2)] \tag{59}$$

$$Z_3(s) = \frac{\alpha_3^2\beta_3 s}{2} + \sum_{n=0}^{\infty}\frac{(-1)^n\varepsilon_n I_n^2(B\alpha_3)}{K_n(\xi\alpha_3)}[\xi\alpha_3 K_{n+1}(\xi\alpha_3) - nK_n(\xi\alpha_3)] \tag{60}$$

$$Z_{12}(s) = \sum_{m=0}^{\infty}\left\{\sum_{n=0}^{\infty}\frac{(-1)^n\varepsilon_n I_n(B\alpha_1)[K_{n-m}(\xi) + K_{n+m}(\xi)]}{K_n(\xi\alpha_1)}\right\}\frac{(-1)^m\varepsilon_m I_m(B\alpha_2)}{K_m(\xi\alpha_2)} \tag{61}$$

$$Z_{13}(s) = \sum_{m=0}^{\infty}\left\{\sum_{n=0}^{\infty}\frac{\varepsilon_n I_n(B\alpha_1)[K_{n-m}(\xi) + K_{n+m}(\xi)]}{K_n(\xi\alpha_1)}\right\}\frac{\varepsilon_m I_m(B\alpha_3)}{K_m(\xi\alpha_3)} \tag{62}$$

For the limiting case where the emitter and receiver rods have zero radius and zero heat capacity, we can replace (56a) with the simpler expression

$$\hat{\Theta}_2^C(s) = \frac{1}{2\pi\tau_0 s} K_0(\xi)\exp(B) \tag{63}$$

which is the dimensionless version of (54). Likewise, we can replace (57a) with the simpler expression

$$\hat{\Theta}_3(s) = \frac{1}{2\pi\tau_0 s} K_0(\xi)\exp(-B) \tag{64}$$

which is the dimensionless version of (55).

Inspection of equations (56) and (57) reveals that the dimensionless rod temperatures $\Theta_2(\tau)$ and $\Theta_3(\tau)$ are functions of eight variables: the dimensionless radii of the three rods, the dimensionless heat capacities of the three rods, the dimensionless heating duration, and the dimensionless variable *B*. However, for the special case where all three rods have the same radius (i.e., $\alpha_1 = \alpha_2 = \alpha_3 = \alpha_0$) and the same heat capacity (i.e., $\beta_1 = \beta_2 = \beta_3 = \beta_0$), we see that $\Theta_2(\tau)$ and $\Theta_3(\tau)$ are functions of only for variables (i.e., α_0, β_0, τ_0, and *B*). Furthermore, upon recognizing that the quantity UL/κ is a sensor-scale Péclet number (i.e., a Péclet number defined using the spacing between the rods as the characteristic length scale), we have $B = Pe/2$ and it follows that $\Theta_2(\tau)$ and $\Theta_3(\tau)$ are functions of α_0, β_0, τ_0, and the sensor-scale Péclet number. The form of equations (63) and (64) reveals that the line-source solutions are functions of only two variables: τ_0 and the sensor-scale Péclet number.

Character of the Solution

A key result evident from the solution $V_2(t)$ is that, if the emitter rod and the downstream receiver rod have identical properties, their finite radius and finite heat capacity have equal influence in modifying

the temperature of the downstream receiver rod. In other words, having an emitter rod of finite radius and a downstream receiver rod of zero radius produces the same result as having an emitter rod of zero radius and a downstream receiver rod of finite radius. This follows from the fact that equations (42) and (43) have the same functional form. A similar result is evident from the solution $V_3(t)$. In that case, if the emitter rod and the upstream receiver rod have identical properties, their finite radius and finite heat capacity have equal influence in modifying the temperature of the upstream receiver rod. This follows from the fact that equations (48) and (49) have the same functional form.

Effect of Finite Radius

The effect of the finite radius of the probes can be seen from the results in Figure A2, where the dimensionless temperature of the downstream and upstream receiver rods is plotted as a function of dimensionless time for three flow rates. In the absence of flow (i.e., *Pe* = 0), the temperatures of the upstream and downstream receiver rods are identical and the results are similar to those in Figure A2 of Knight et al. (2012). Comparing the curves for $\alpha_0 = 0.05$, $\alpha_0 = 0.1$, and $\alpha_0 = 0.15$ with the line-source solution for this zero-flow case shows that the finite radius of the rods causes the heat-pulse signal to arrive at the receiver rods slightly earlier in time. This time shift is caused by the fact that the effective distance traveled by the heat-pulse signal is smaller when the rods have a finite radius. As expected, this effective travel distance decreases as rod radius increases.

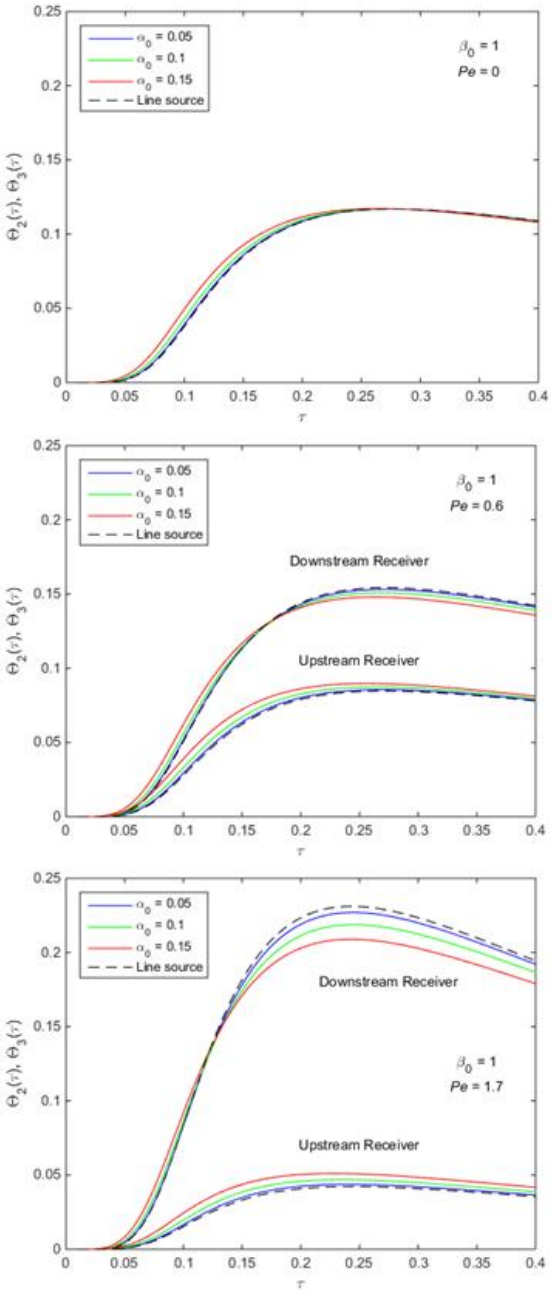

Figure A2. Dimensionless temperatures Θ_2 and Θ_3 of the downstream receiver and upstream receiver rods, respectively, as functions of dimensionless time τ for Péclet numbers of *Pe* = 0, 0.6, and 1.7. Results are from (56) and (57) with a dimensionless heating duration of τ_0 = 0.05, a dimensionless rod heat capacity of β_0 = 1, and dimensionless rod radii of α_0 = 0.05, 0.10, and 0.15. Results for the line-source solution are from the inversion of (63) and (64). The temperatures of the downstream and upstream receiver rods are identical in the absence of flow (i.e., *Pe* = 0).

In the presence of flow (*Pe* > 0), the finite radius of the rods produces an effect similar to that in the absence of flow, at least for relatively early times ($0 < \tau < 0.125$). That is, for both upstream and

downstream receiver rods, it causes the heat-pulse signal to arrive slightly earlier in time. But the finite radius of the rods also has a marked effect on the maximum temperature rise. For the downstream receiver, the maximum temperature rise decreases as the finite radius of the rods increases. For the upstream receiver, the maximum temperature rise increases as the finite radius of the rods increases. Inasmuch as the method of Ren et al. (2000) is based on the maximum temperature difference between the upstream and downstream receiver rods, it is clear from our results that the sensitivity of their method likely would decrease as rod radius increases.

Effect of Finite Heat Capacity

The effect of the finite heat capacity of the probes can be seen from the results in Figure A3, where the dimensionless temperature of the downstream and upstream receiver rods is plotted as function of dimensionless time for three flow rates. In the absence of flow (i.e., *Pe* = 0), the temperatures of the upstream and downstream receiver rods are identical and the results are similar to those in Figure A3 of Knight et al. (2012). The influence of the finite heat capacity of the rods for this zero-flow case can be understood by comparing the curves for $\beta_0 = 0.5$ and $\beta_0 = 2$ with the curve for $\beta_0 = 1$. Relatively less energy is needed to raise the temperature of the receiver rods when $\beta_0 < 1$. This causes an increase in the magnitude of the heat-pulse signal, and the signal is positively skewed so that the maximum temperature rise occurs earlier. Conversely, relatively more energy is needed to raise the temperature of the receiver rods when $\beta_0 > 1$. As a result, the magnitude of the heat-pulse signal decreases and the signal is negative skewed so that the maximum temperature rise occurs later.

In the presence of flow (*Pe* > 0), the effect of the finite heat capacity of the rods appears to be more pronounced for the downstream receiver rod and less pronounced for the upstream receiver rod. This is most likely due to the fact that, for *Pe* > 0, the temperature rise is greater in magnitude for the

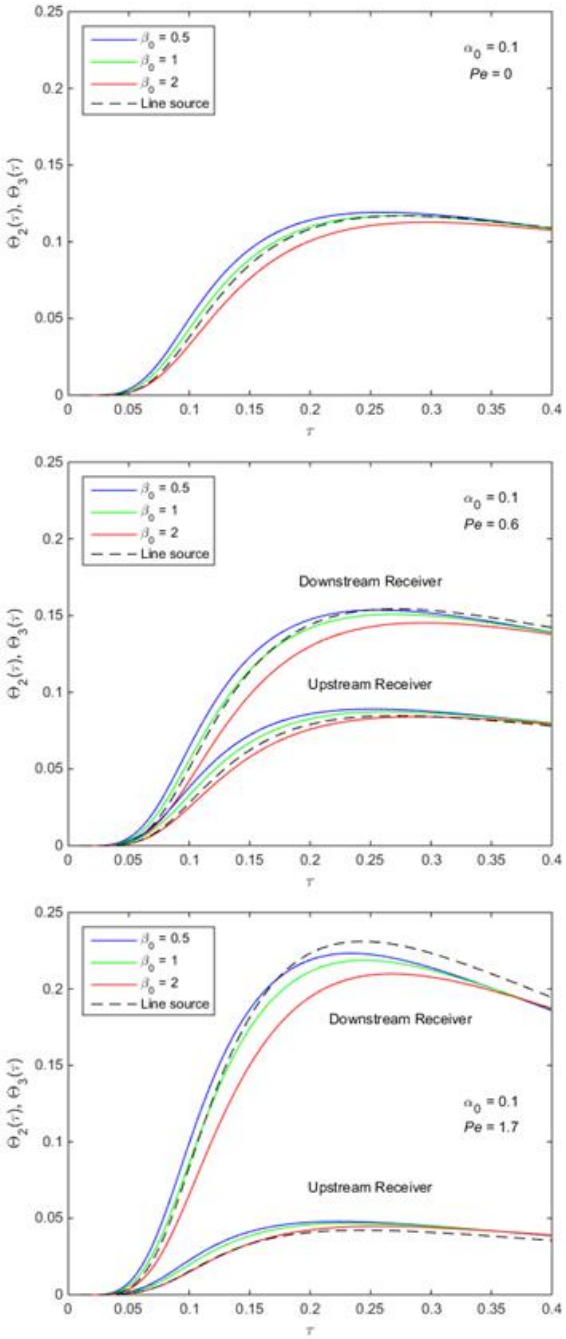

Figure A3. Dimensionless temperatures Θ_2 and Θ_3 of the downstream receiver and upstream receiver rods, respectively, as functions of dimensionless time τ for Péclet numbers of *Pe* = 0, 0.6, and 1.7. Results are from (56) and (57) with a dimensionless heating duration of τ_0 = 0.05, a dimensionless rod radius of α_0 = 0.1, and dimensionless rod heat capacities of β_0 = 0.5, 1, and 2. Results for the line-source solution are from the inversion of (63) and (64). The temperatures of the downstream and upstream receiver rods are identical in the absence of flow (i.e., *Pe* = 0).

downstream receiver and smaller in magnitude for the upstream receiver. And we expect rod heat

capacity effects to scale according to the magnitude of the temperature rise.

Results for a Typical Sensor

Here we present results for a typical sensor in terms of dimensioned variables. The results are for a sensor having three rods, each with a radius of $a_0 = 6.35 \times 10^{-4}$ m. The three rods are equally spaced, with a rod spacing of $L = 6.0 \times 10^{-3}$ m. Thus, the ratio of the rod radius and rod spacing is $\alpha_0 = a_0/L$ = 0.105833. The heat capacity of the rods was calculated by using the expression

$$C_0 = \left(\frac{a_e}{a_0}\right)^2 C_e + \left[1 - \left(\frac{a_e}{a_0}\right)^2\right] C_{ss} \tag{65}$$

where a_e is the radius of the epoxy-filled region within the rods, C_e is the volumetric heat capacity of the thermally conductive epoxy, and C_{ss} is the volumetric heat capacity of stainless steel. The results presented here were obtained using the values $a_e = 4.19 \times 10^{-4}$ m, $C_e = 1.64$ MJ m^{-3} K^{-1}, and C_{ss} = 3.77 MJ m^{-3} K^{-1} from Knight et al. (2012). When used in equation (65), these values yield the result C_0 = 2.842615 MJ m^{-3} K^{-1} for the volumetric heat capacity of the rods. All results were generated using a heating rate of q' = 100 W m^{-1}, a heating duration of t_0 = 8 s, and the thermal properties C = 3.07 MJ m^{-3} K^{-1} and λ = 1.95 W m^{-1} K^{-1} for a water-saturated Hanlon sand (Knight et al., 2012). For this combination of soil and sensor, the ratio of the rod and soil heat capacities is $\beta_0 = C_0/C$ = 0.925933. Results were generated for soil water flux densities of J = 0, 100, and 1,000 cm d^{-1}, which correspond to thermal front advection velocities of U = 0, 1.575884×10^{-5} and 1.575884×10^{-4} m s^{-1}. They also correspond to Péclet numbers of Pe = 0, 1.488604×10^{-1}, and 1.488604 when the heat capacity of water is taken to be C_w = 4.18 MJ m^{-3} K^{-1}.

As expected, the results for this combination of soil and sensor (Figure A4) show the same general behavior as the results in Figures A2 and A3. The temperatures of the upstream and downstream receiver rods are identical for the case of zero flow (i.e., $Pe = 0$). But as the soil water flux increases, the temperature rise of the upstream receiver rod decreases and the temperature rise of the downstream receiver rod increases. The results also show that deviation between the line-source solution and solutions V_2 and V_3 clearly become greater as the soil water flux density increases.

Summary and Next Steps

The method of Ren et al. (2000) for measuring soil water flux density is based on a line-source solution that does not account for the finite radius and finite thermal properties of the sensor's rods. In this report, we derive solutions that partially account for the finite properties of the emitter and two receiver rods. Specifically, we have derived Laplace-domain solutions for the temperature of the receiver rods directly downstream and directly upstream from the emitter. These solutions only partially account for the finite properties of the emitter and receiver rods because they were derived by assuming that the rods behave like cylindrical perfect conductors. The solutions are more difficult to evaluate than the line-source solution of Ren et al. (2000); however, compared to the line-source solution, little additional time is required to complete the evaluation. Thus, from a computational perspective, the solutions derived in this report have the desirable property that they could replace the line-source solution in the flux estimation method of Ren et al. (2000). What remains to be determined is whether or not the new solutions improve upon the accuracy of flux estimates obtained with the simpler line-source solution.

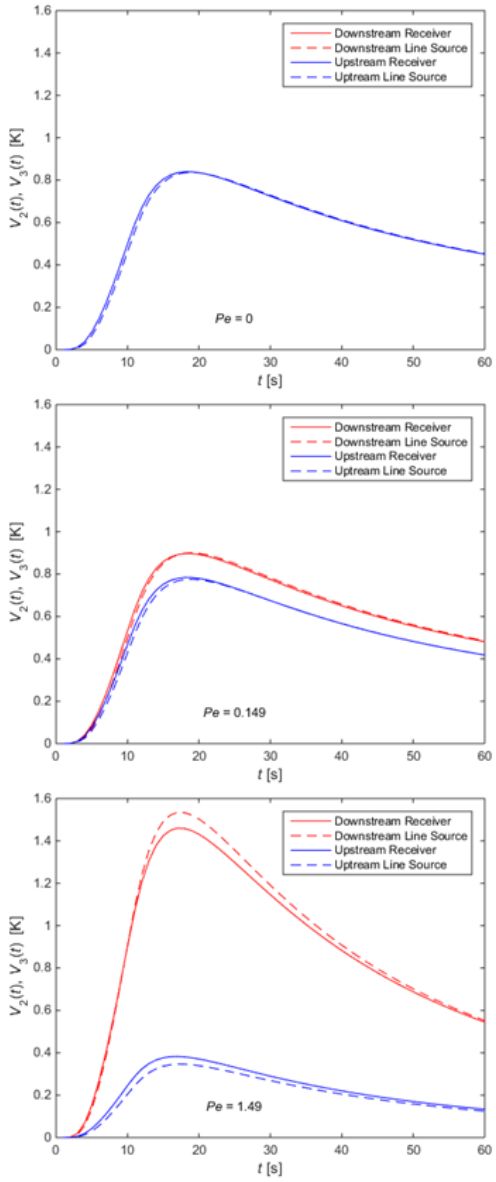

Figure A4. Temperatures V_2 and V_3 of the downstream receiver and upstream receiver rods, respectively, as functions of time *t* for Péclet numbers of *Pe* = 0, 0.149 and 1.49. Results are from (52) and (53) with a heating rate of q' = 100 W m^{-1} and a heating duration of t_0 = 8 s. The results were obtained using the following rod and soil properties: a_0 = 6.35 × 10^{-4} m, *L* = 6.0 × 10^{-3} m, C_0 = 2.842615 MJ m^{-3} K^{-1}, *C* = 3.07 MJ m^{-3} K^{-1}, and λ = 1.95 W m^{-1} K^{-1}. Results for the line-source solution are from the inversion of (54) and (55). The temperatures of the downstream and upstream receiver rods are identical in the absence of flow (i.e., *Pe* = 0).

Nomenclature

Coordinate systems

(x, y)	Cartesian coordinate system centered on the emitter rod
(r_1, θ_1)	polar coordinate system centered on the emitter rod
(r_2, θ_2)	polar coordinate system centered on the receiver rod

Other variables and constants

a_0	radius of the rods for the case where all three rods have the same radius [m]
a_1, a_2, a_3	radii of the emitter, downstream receiver, and upstream receiver rods [m]
a_e	radius of the epoxy-filled region in the rods [m]
b	constant [m^{-1}], defined as $b = U/(2\kappa)$
c_n	indexed coefficient in the Laplace-domain solution centered at the emitter
B	dimensionless constant, defined as $B = bL = UL/2\kappa$
C	volumetric heat capacity of the bulk porous medium [J m^{-3} K^{-1}]
C_e	volumetric heat capacity of thermally conductive epoxy [J m^{-3} K^{-1}]
C_{ss}	volumetric heat capacity of stainless steel [J m^{-3} K^{-1}]
C_w	volumetric heat capacity of water [J m^{-3} K^{-1}]
C_0	volumetric heat capacity of the rods for the case where all three rods have the same heat capacity [J m^{-3} K^{-1}]
C_1, C_2, C_3	volumetric heat capacities of the emitter, downstream receiver rod, and upstream receiver rods [J m^{-3} K^{-1}]
d_m	indexed coefficient in the Laplace-domain solution centered at the receiver
f	arbitrary function of time used to define the Laplace transform of a function
$I_n(\ )$	modified Bessel function of the first kind and order *n*
J	volumetric flux density of water [m^3 m^2 s^{-1}]
$K_n(\ )$	modified Bessel function of the second kind and order *n*
L	distance between the centerlines of the emitter and receiver rods [m]
m,*n*	integers
p	Laplace transform variable [s^{-1}]
Pe	Péclet number [-], defined as $Pe = UL/\kappa$
q′	rate per unit length of heat released from the emitter rod [W m^{-1}]
s	dimensionless Laplace transform variable, defined as $s = p\kappa/L^2$
t	time [s]
t_0	heating duration [s]
u	modified temperature of the porous medium [K], defined as $u \equiv \upsilon \exp(-bx)$

U	thermal front advection velocity [m s^{-1}]
U_w	velocity of water in the porous medium [m s^{-1}]
V_1, V_2, V_3	temperatures of the emitter, downstream receiver and upstream receiver rods [K]
α_0	dimensionless radius of the rods for the case where all three rods have the same radius, defined as $\alpha_0 = a_0/L$
$\alpha_1, \alpha_2, \alpha_3$	dimensionless radii of the emitter, downstream receiver, and upstream receiver rods, defined as $\alpha_1 = a_1/L$, $\alpha_2 = a_2/L$, and $\alpha_3 = a_3/L$
β_0	ratio of the rod and porous medium volumetric heat capacities for the case where all three rods have the same heat capacity [-], defined as $\beta_0 = C_0/C$
$\beta_1, \beta_2, \beta_3$	dimensionless heat capacity ratios, defined as $\beta_1 = C_1/C$, $\beta_2 = C_2/C$, $\beta_3 = C_3/C$
$\varepsilon_m, \varepsilon_n$	indexed constants [-] that are assigned integer values of either 1 or 2.
Θ_2, Θ_3	dimensionless temperatures of the downstream and upstream receiver rods, defined as $\Theta_2 = CL^2V_2/(q't_0)$, $\Theta_3 = CL^2V_3/(q't_0)$
ϑ	volumetric water content of the porous medium [m^3 m^{-3}]
κ	thermal diffusivity of the bulk porous medium [m^2 s^{-1}], defined as $\kappa = \lambda/C$
λ	thermal conductivity of the bulk porous medium [W m^{-1} K^{-1}]
μ	coefficient [m^{-2}], defined as $\mu^2 = b^2 + p/\kappa$
ξ	dimensionless coefficient, defined as $\xi = \mu L$, $\xi^2 = B^2 + s$
τ	dimensionless time, defined as $\tau = \kappa t/L^2$
τ_0	dimensionless heating duration, defined as $\tau_0 = \kappa t_0/L^2$
υ	temperature of the porous medium [K]
ϕ	arbitrary heating function for the emitter rod; a function of time specifies the rate per unit length at which heat is released from the emitter rod

Appendix B: A Numerical Solution for Data Assimilation

Temperature data are generate using a finite-element model that accounts for the thermal properties of all the materials and the flow around the probes (Scenario 5, Table 1). Using this complexity level we simulated two sensor designs:

- The conventional heat-pulse (HP) sensor with probes of 1.27 mm diameter and 6 mm center-to-center spacing.
- The rigid HP (R-HP) sensor with probes of 2.38 mm diameter and 7 mm center-to-center spacing (Figure 1).

The simulations included:

- Four saturation levels: 10, 20, 30, and 37.1% volumetric water content (VWC), with the latter being the saturated case.
- Eight WFD magnitudes: 1, 5, 10, 50, 100, 200, 500, and 1000 cm/d.

Estimation of Water Flux Density (WFD)

The assimilated temperature data is used as temperature observations for fitting the analytical models: ILS and perfect conductors (Appendix A). For fitting, we assume that the thermal properties and center-to-center probe spacing are known, and optimize the WFD.

Figure B1 presents an example of assimilated results and the fit of the perfect conductors model (ILS not shown.

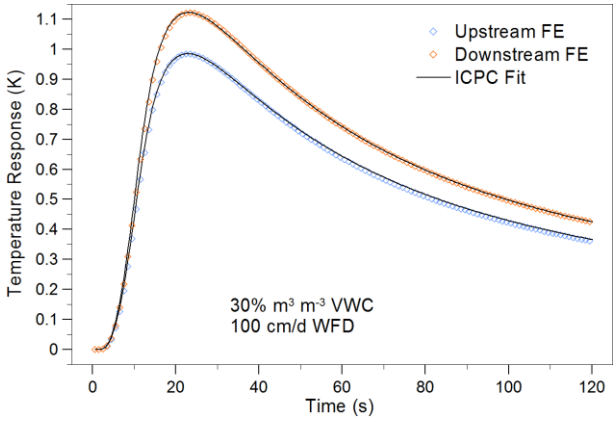

Figure B1. Upstream (blue) and Downstream (red) results of the finite element (FE) model and their fit with the perfect conductors model. The results were generated with simulation conditions of 30% VWC and 100 cm/d WFD.

Figure B2 depicts the WFD estimation accuracy, comparing assimilated (applied) WFD and estimated ones. Estimations of WFD are significantly improved with the perfect conductors

model. Both, ILS and perfect conductors models underestimate WFD. However, these underestimations are more significant with the ILS model.

As the soil gets drier, the underestimation with the ILS model is more significant. However, the estimations with the perfect conductors model improve in drier conditions. We attribute that to difference between the heat capacity of the soil and the probes. That difference is larger in drier conditions, which increases the underestimations in the ILS model, because there are no probes in that model. However, because the perfect conductors model accounts for the heat capacity, estimations improve with that model.

The other noticeable difference is the change in WFD underestimations of data that was collected from simulations of the conventional HP sensor and the rigid HP sensor. Comparing estimations of either ILS or perfect conductors models, the underestimations of the conventional HP sensor (Figure B2, left side) are less significant than those of the rigid HP sensor. We attribute these differences to the size of the probes. Obviously, the ILS model, which does not account for the probes, underestimates WFD as the probes are larger. However, even in the perfect conductors model the underestimations are more significant in the R-HP sensor. We attribute that to the flow of water around the probes. The perfect conductors model considers uniform (unidirectional) flow, so it does not account for heat that is convected perpendicular to the probe alignment. Therefore, the heat that is convected away with the numerical FE is interpreted as lower WFD with that analytical perfect conductors model.

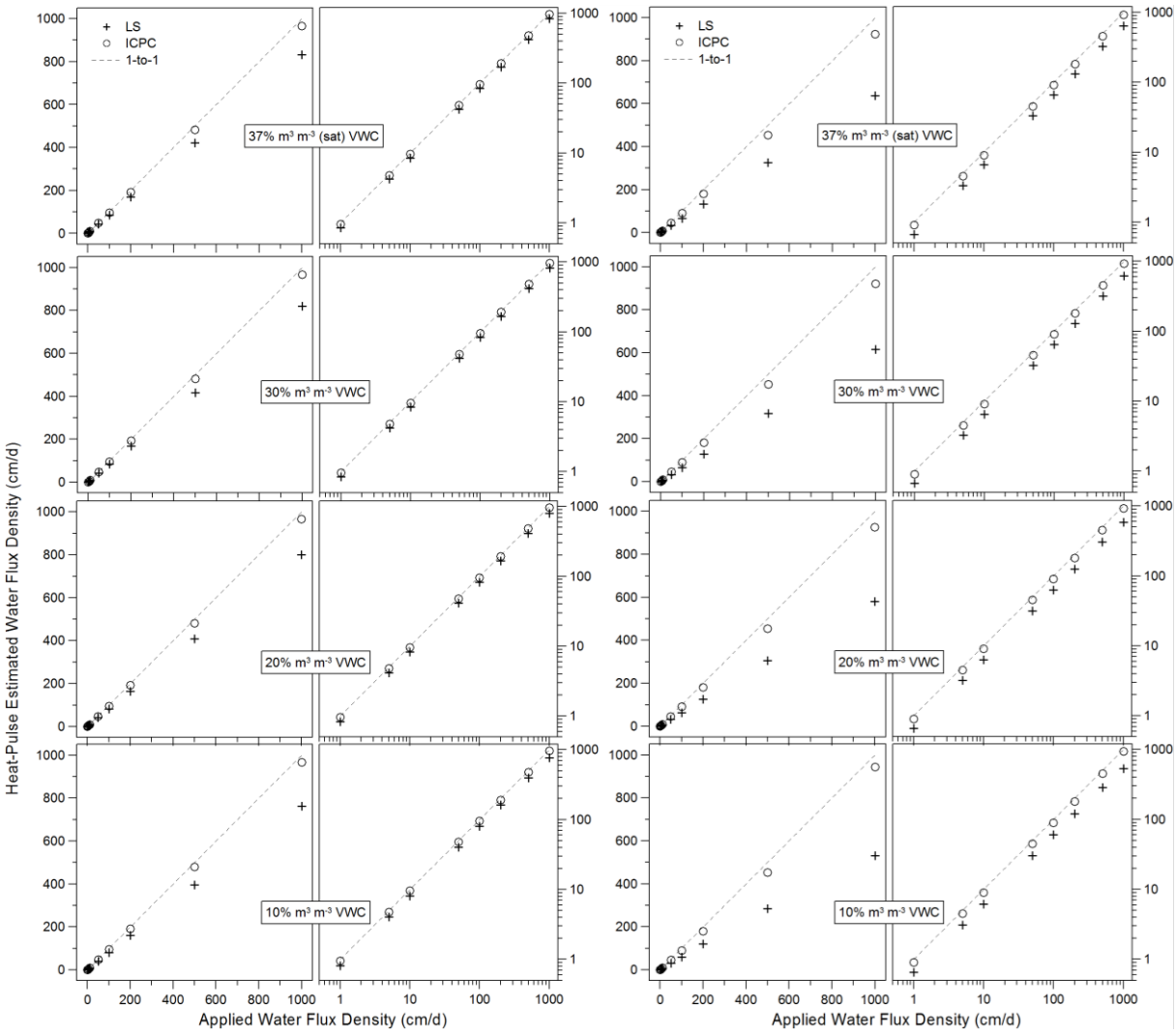

Figure B2. WFD estimations from the conventional HP (left plots) and the R-HP (right plots). Each set of plots (left and right) are presents in linear and log-log scales. Each row represents different water content, with WFD estimations conducted with the ILS and perfect conductors models.

References

Carslaw, H.S., and J.C. Jaeger. 1959. Conduction of heat in solids. 2nd ed. Oxford Univ. Press, London.

Kamai, T., Tuli, A., Kluitenberg, G.J., and Hopmans, J.W. (2008). Soil Water Flux Density Measurements near 1 cm d(-1) using an Improved Heat Pulse Probe Design. Water Resources Research. 44. doi: 10.1029/2008wr007036.

Kamai, T., Kluitenberg, G.J., and Hopmans, J.W. (2015). A Dual-Probe Heat-Pulse Sensor with Rigid Probes for Improved Soil Water Content Measurement. Soil Science Society of America J., doi:10.2136/sssaj2015.01.0025.

Knight, J.H., G.J. Kluitenberg, and T. Kamai. 2016. The dual-probe heat-pulse method: Interaction between probes of finite radius and finite heat capacity. J. Eng. Math. 99:79-102, doi 10.1007/s10665-015-9822-x.

Knight, J.H., G.J. Kluitenberg, T. Kamai, and J.W. Hopmans. 2012. Semianalytical solution for dual-probe heat-pulse applications that accounts for probe radius and heat capacity. Vadose Zone J. 11(2), doi:10.2136/vzj2011.0112.

Marshall, D.C. 1958. Measurement of sap flow in conifers by heat transport. Plant Physiol. 33:385–396.

Melville, J.G., F.J. Molz, and O. Güven. 1985. Laboratory investigation and analysis of a ground-water flowmeter. Ground Water 23:486–495.

Olver, F.W.J. 1965. Bessel functions of integer order. p. 355–433. *In* M. Abramowitz and I.A. Stegun (ed.) Handbook of mathematical functions with formulas, graphs, and mathematical tables. Dover, New York.

Ren, T., G.J. Kluitenberg, and R. Horton. 2000. Determining soil water flux and pore water velocity by a heat pulse technique. Soil Sci. Soc. Am. J. 64:552–560.

Stehfest, H. 1970a. Algorithm 368: Numerical inversion of Laplace transforms [D5]. Commun. ACM 13:47–49.

Stehfest, H. 1970b. Remark on Algorithm 368 [D5]: Numerical inversion of the Laplace transforms. Commun. ACM 13:624.